PCCP
Physical Chemistry Chemical Physics

Accepted Manuscript

This article can be cited before page numbers have been issued, to do this please use: Y. Velázquez-Galván and A. Encinas, *Phys. Chem. Chem. Phys.*, 2020, DOI: 10.1039/D0CP00808G.

ROYAL SOCIETY OF CHEMISTRY

rsc.li/pccp

View Article Online
DOI: 10.1039/D0CP00808G
ROYAL SOCIETY OF CHEMISTRY

Journal Name

ARTICLE TYPE

Cite this: DOI: 10.1039/xxxxxxxxxx

Analytical magnetostatic model for 2D arrays of interacting magnetic nanowires and nanotubes

Yenni Velázquez-Galván[†], and Armando Encinas[*]

Received Date
Accepted Date

DOI: 10.1039/xxxxxxxxxx

www.rsc.org/journalname

A fully analytical model to describe the magnetostatic properties of these 2D nanocylinder arrays (tubes and wires) is presented. The model allows calculating the components of the effective demagnetizing field as a function of the cylinder height, inner and outer diameters, and the center-to-center distance. From these components, it is possible to calculate the shape anisotropy of the cylinder, the dipolar interaction between them, and the total magnetostatic energy. The model allows performing calculations very simply, using a simple spreadsheet or open-access software such as Geogebra. This allows analyzing the effect of each geometrical parameter in the different contributions to the magnetostatic energy. Amongst the most interesting findings is that the model describes naturally the magnetization easy-axis reorientation transition induced by the dipolar interaction, for which a general phase diagram has been calculated for both tubes and wires. For the case of nanowires, our results show a very good agreement with previously published results. While for nanotubes, the model predicts that the magnetization easy-axis reorientation transition is frustrated as the tube wall thickness decreases and reaches a critical value even when the distance between tubes is reduced to its lowest possible value.

1 Introduction

Magnetic nanostructures are currently of great scientific and technological interest. Over the last three decades, these materials have demonstrated a wealth of important effects related to their size and shape and have lead to significant scientific breakthroughs[1,2]. Important application domains include 3D magnetic nanostructures,[3,4] high-density magnetic recording media[5,6], spintronics[7], spincaloritronics[8–10], sensors[11], nanomagnetic logic[12], frustrated nanomagnetics and artificial spinice[13], nanobiomedicine[14–17] as well as magnetoelectric energy conversion systems[18–20]. Two-dimensional arrays of magnetic Nanowires (NW) and Nanotubes (NT) have received considerable interest both for their fundamental properties as well as the great potential shown for numerous applications[21–24]. Central to the advantageous features of these 2D arrays is the uniaxial shape anisotropy of these needle-shaped nanomagnets, which in conjunction with the inter-particle dipolar interaction are largely responsible for the vast and complex magnetic properties of these assemblies.[21–25] While other coupling or anisotropy effects may contribute to the overall magnetic properties of the assembly, shape anisotropy and the dipolar interaction are of crucial importance because they are always present, and in most cases, they compete or overshadow other contributions to the total magnetic energy.[23–27] Furthermore, they are both of magnetostatic origin and their main properties depend directly on the geometrical parameters of the system.

The modeling of these systems has been done at several approximation levels. Micromagnetic simulations have been extensively used to model NW as well as NT arrays[28–33]. Some inconveniences of these methods are that they require some degree of programming specialization; the source code is generally not accessible or friendly for its modification or adaptation to specific conditions. Computing resources and computing time are also a common concern. Moreover, modeling particle assemblies is also difficult and often requires using approximations or simplifications of the system in order to avoid excessive computing requirements.

Other models to describe NW and NT arrays have also been proposed. Some of these models are analytical[34], while other models consider the NW or NTs formed by a large number of smaller elemental particles with well-known magnetic properties and magnetization reversal mechanisms[35–39]. These methods have allowed obtaining valuable information about the magnetization reversal properties for individual wires and tubes. How-

División de Materiales Avanzados, Instituto Potosino de Investigación Científica y Tecnológica, Caminio a la Presa San José 2055, 78216 San Luis Potosí, SLP, Mexico.
[†] *Present address: Departamento de Matemáticas y Física, Instituto Tecnológico y de Estudios Superiores de Occidente, Periférico Sur Manuel Gómez Morín 8585, 45604 Tlaquepaque, Jalisco, Mexico*
[*] *E-mail: armando.encinas@ipicyt.edu.mx*

ever, with a singular exception,[37] their applicability to arrays in which interaction effects are present, has not been considered or is limited to a few interacting particles. Similarly to micromagnetic modeling, the description of particle assemblies and interaction effects is difficult and limited.

Mean-field models have also been proposed in order to take into account both shape anisotropy and dipolar interaction in NW[40–42], as well as NT[34,43] arrays. These mean-field models have gained some interest since they can provide results easily and without the need for specialized computing knowledge or infrastructure. However, depending on the different approximations used, the complexity of the calculations may vary, thus limiting the full description of the magnetic properties. For example, a well known effect in NW arrays is the Easy Axis Reorientation Transition (EART) induced by the dipolar interaction, has been described for some particular cases for NWs,[40,44] while there are no reports at present of these effects in NT arrays.

In this sense, different modeling approaches are needed to provide a more detailed, complete and accurate description of the magnetic properties of NW and NT arrays that do not require specialized computing hardware or specific and advanced programming skills. In particular, regarding the interplay between shape anisotropy and dipolar interaction in assemblies formed by a large number of particles and their dependence on all the geometrical parameters of the system.

Herein we propose a simple mean-field analytical model that incorporates the contributions of the shape anisotropy and the dipolar interaction for arrays of NWs and NTs. This model depends on all the geometrical parameters of the system, and their individual effects can be easily modeled. The model relies on a single equation that can be computed using non-specialized software and, therefore, does not require any advanced programming skills. Furthermore, as we show here, calculations can be done using the freeware GeoGebra[45] on any computer, tablet, or Smartphone. We show that the model provides accurate results for both the shape anisotropy as well as for the dipolar interaction for both NW and NT arrays. Analyzing the interplay between shape anisotropy and dipolar interaction, we also derive an analytical expression for the easy axis reorientation transition induced by the dipolar interaction, which has been studied as a function of the interwire distance, NW (NT) aspect ratio and the NT wall thickness. For NT arrays, the model predicts that reducing the NT wall thickness, even as the inter-tube distance is reduced to its minimum value, can frustrate the EART. This effect is analyzed in detail, and a phase diagram has been obtained as a function of the reduced inner-radii and the NT aspect ratio.

2 Magnetostatic model for a 2D array of nanotubes

First the expressions for the effective demagnetizing field and the effective magnetic anisotropy are presented. These expressions follow from a mean-field model presented in a previous report[46] which has already been applied to study the dipolar interaction effects in a 2D array of magnetic nanotubes[43]. However, herein we use the approximate expression for the demagnetizing factor

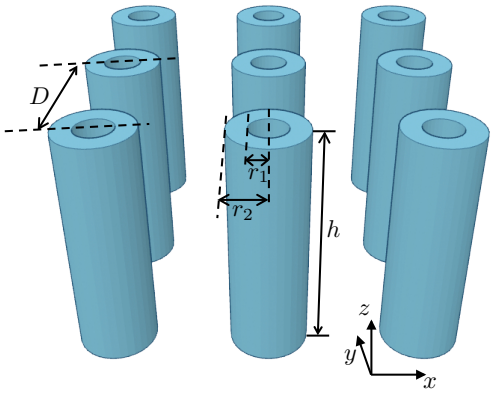

Fig. 1 Schematics of a nanotube array, showing the NT height h, inner and outer radii, r_1 and r_2, respectively as well as the center to center distance between nanotubes D. The outer diameter is $\phi = 2r_2$ so their aspect ratio is $\tau = h/\phi$, the reduced center to center distance is $d = D/\phi$ and the ratio between the inner and outer radii, or the reduced inner radii $\beta = r_1/r_2$.

of the circular cylinder proposed by Sato and Ishii[47] allowing to obtain analytical expressions for the effective anisotropy of the NT array.

Consider an infinite 2D hexagonal array of identical NTs assumed to be homogeneously magnetized. As shown in Figure 1, the NTs have their long axes parallel and aligned along the z-axis. The NTs array is described by their height (h), the center-to-center distance (D) and their inner and outer radii r_1 and r_2, respectively. Equivalently their inner and outer diameter, $\phi_i = 2r_1$ and $\phi = 2r_2$ can also be used. For convenience, we normalize all these quantities by the outer diameter; then, we have the NT aspect ratio, or reduced height ($\tau = h/\phi$), the reduced center to center distance ($d = D/\phi$), and the reduced inner radii ($\beta = \phi_i/\phi = r_1/r_2$). In the following, these three reduced parameters will be simply referred to as the aspect ratio, center-to-center distance, and reduced inner radii. For a two dimensional hexagonal array, the packing fraction is given by,

$$P_0 = \frac{\pi}{2\sqrt{3}}\left(\frac{1}{d^2}\right) \tag{1}$$

This definition of the packing fraction is only related to the external radii and does not include the volume difference related to the cavity of the tubes. Taking this volume into account, the packing fraction of an assembly of NTs is[43],

$$P = P_0(1-\beta^2) \tag{2}$$

For an assembly of identical particles, the effective demagnetizing factor N_{eff} can be expressed as a combination of the demagnetizing factors of the individual particles N and the volume that contains the whole assembly N^+ and the packing fraction P of the particles in this volume. In particular,[46]

$$N_{eff} = N + (N^+ - N)P \tag{3}$$

The effective magnetic anisotropy energy density is defined as,[43,46]

$$E_K = \frac{1}{2}\mu_0 M_s^2 \Delta N_{eff} \tag{4}$$

View Article Online
DOI: 10.1039/D0CP00808G

where $\Delta N_{eff} = N^y_{eff} - N^z_{eff}$. From equation (3) this leads to the following expression,

$$E_K = \frac{1}{2}\mu_0 M_s^2 \left[\Delta N + (\Delta N^+ - \Delta N)P\right] \quad (5)$$

The coefficient on the right-hand side of this expression is constant, so for convenience in the following we will use reduced quantities: reduced effective anisotropy energy, $\mathscr{E}_K = 2E_K/(\mu_0 M_s^2)$, reduced shape anisotropy $\mathscr{E}_S = 2E_S/(\mu_0 M_s^2)$, and reduced dipolar interaction energy $\mathscr{E}_{Dip} = 2E_{Dip}/(\mu_0 M_s^2)$.

For a cylindrical tube with a circular cross-section, $N = \{N_y, N_y, N_z\}$. For an infinite 2D array, the external volume can be approximated as a thin film whose thickness is much smaller than the lateral dimensions. In this case, the demagnetizing factor is $N^+ = \{0,0,1\}$. By inserting these values into Eq. (3), the components of the effective demagnetizing factor along the tube axis and perpendicular to it are,

$$N^z_{eff} = N_z + (1-N_z)P \quad (6)$$

$$N^y_{eff} = N_y - N_y P \quad (7)$$

The reduced anisotropy energy follows from using these expressions in Eq. (5), which can be further simplified by taking into account that the trace of the demagnetizing factor is a constant. Using $N_z + 2N_y = 1$, the reduced anisotropy energy can be written solely in terms of N_z, in particular,

$$\mathscr{E}_K = \left[\frac{1}{2} - \frac{3}{2}N_z\right] - \left[\frac{3}{2}(1-N_z)P\right]. \quad (8)$$

This expression of the effective anisotropy energy has two contributions, the first term corresponds to the shape anisotropy of a single NT ($\mathscr{E}_S$) while the second term that depends on the packing fraction represents the dipolar interaction between the NTs ($\mathscr{E}_{Dip}$), this is $\mathscr{E}_K = \mathscr{E}_S - \mathscr{E}_{Dip}$, where the negative sign indicates that the interaction is antiferromagnetic. The reduced effective anisotropy energy depends only on the axial component of the demagnetizing factor of the NT, which can be computed using the expression proposed by Nam et al.,[48] that relates the axial demagnetizing factor of the tube, N_z, with that of the cylinder (or wire), N_{wz}

$$N_z = N_{wz}(1-\beta^2) \quad (9)$$

While the axial demagnetizing factor of a single cylinder is computed as a function of the aspect ratio $\tau = h/\phi$ using the approximate expression proposed by Sato and Ishii[47], namely.

$$N_{wz} = \frac{1}{1+\frac{4\tau}{\sqrt{\pi}}} \quad (10)$$

Substitution of these expressions in Eq. (8) for N_z and Eqs. (1) and (2) for P leads to an explicit equation for the reduced effective anisotropy energy as a function of the NT aspect ratio, center-to-center distance and reduced inner radii,

$$\mathscr{E}_K = \frac{3}{2}\left(\frac{1}{3} - \frac{(1-\beta^2)}{1+\frac{4\tau}{\sqrt{\pi}}}\right) - \frac{\pi\sqrt{3}}{4}\left(1 - \frac{(1-\beta^2)}{1+\frac{4\tau}{\sqrt{\pi}}}\right)\frac{(1-\beta^2)}{d^2} \quad (11)$$

The equation is written so that the first term corresponds to the shape anisotropy of a single non-interacting NT and the second term is the dipolar interaction. The first term depends only on the NT aspect ratio and the reduced inner radii, whereas the second term also depends on these two quantities and also on the reduced center-to-center distance. Using this expression, it is simple and practical to calculate each contribution and the reduced effective anisotropy energy without requiring extensive computing efforts.

A first analysis of Eq (11) shows that the corresponding expression for NW arrays is obtained when the inner radii vanishes, $\beta = 0$. Indeed, writing $(\pi\sqrt{3})/4$ as $(3/2)\pi/(2\sqrt{3})$ in the second term, we recover Eq.(8) for N_{wz} instead of N_z, which corresponds to the reduced effective anisotropy of a NW array of arbitrary aspect ratio[46]. Furthermore, in the limiting case of very high aspect ratio NWs ($N_{wz} = 0$) Eq. (11) reduces to well-known expression for infinitely tall wires[40],

$$\mathscr{E}_K = \frac{1}{2} - \frac{3}{2}P_0 \quad (12)$$

3 Effective magnetic anisotropy of nanowires and nanotubes

Equation (11) describes the effective anisotropy in an array of NTs. The first term corresponds to the shape anisotropy of a single (non-interacting) NT ($\mathscr{E}_S$). Figure 2 (a) shows the variation of this shape anisotropy as a function of the aspect ratio for different values of β. Starting with the particular case of a single nanowire ($\beta = 0$) we see the well known variation of the shape anisotropy with the aspect ratio. High aspect ratios result in an easy axis along the wire axis ($\mathscr{E}_S > 0$), while low aspect ratios result in an easy axis perpendicular to the wire axis ($\mathscr{E}_S < 0$). There is a critical aspect ratio for which the anisotropy vanishes ($\mathscr{E}_S = 0$). For nanotubes ($\beta > 0$), we see that the shape anisotropy is always larger than for the corresponding NW having the same aspect ratio, and, as the NT wall thickness decreases (β increases), this difference becomes larger. As a consequence, we can see that the critical aspect ratio (τ_c) at which the easy axis rotates from parallel to perpendicular to the NT axis shifts towards lower values as β increases. Moreover, as seen in the figure, above a certain value of β, the easy axis no longer rotates from parallel to perpendicular. This value can be obtained by equating to zero the first term in Eq. (11) and solving for τ_c. This is,

$$\tau_c = \frac{3\sqrt{\pi}}{4}\left(\frac{2}{3} - \beta^2\right) \quad (13)$$

This expression shows the relation between the critical aspect ratio and the NT wall thickness, where it is seen that as β^2 increases, τ_c decreases. Furthermore, since $\tau \geq 0$ it follows that this requires that $\beta^2 \leq 2/3$. Hence, for $\beta^2 > 2/3$, or $\beta > 0.8164$; the easy axis reversal can not take place. In other words, for a single non-interacting NT, the effective demagnetizing field along the NT axis will always be smaller than the one along the direction perpendicular to the NT axis if $\beta > 0.8164$.

Figure 2 (b) shows the dipolar interaction energy ($\mathscr{E}_{Dip}$) as a function of the reciprocal reduced center-to-center distance

View Article Online
DOI: 10.1039/D0CP00808G

($1/d = \phi/D$) for NT with a fixed aspect ratio of τ=10 and for different values of the tube wall thickness. Considering first the limiting case of the NW ($\beta = 0$), we see that the dipolar interaction energy goes to zero when the center-to-center distance is large, $1/d \to 0$, and it increases when this distance decreases, tending to its maximum value as $1/d \to 1$. For NTs ($\beta > 0$), the behavior is similar, but as seen in the figure, as the NT wall thickness decreases (β increases), the corresponding curves shift downwards. This shift is consistent with a reduction of the interaction field in NTs with respect to NWs as the tube wall thickness decreases, which is related to the decrease of the packing fraction as expressed by Eq. (2)[43].

The results for the shape anisotropy, Fig. 2 (a), and the dipolar interaction, Fig. 2 (b), show that the presence of the cavity in the tube leads to a reinforcement of the shape anisotropy and a reduction of the dipolar interaction with respect to the wire geometry. These effects compete to determine the effective magnetic anisotropy ($\mathscr{E}_K$) as shown in figure 2 (c) where $\mathscr{E}_K$ as a function of the reciprocal reduced center-to-center distance ($1/d$) for NT with a fixed aspect ratio of τ=10 and for different values of the tube wall thickness is shown.

As seen in the figure, regardless of the value of β, the effective magnetic anisotropy decreases as the distance between NTs is reduced ($1/d \to 1$) as a consequence of the competition between the shape anisotropy and the antiferromagnetic dipolar interaction. As expected, when the tubes are infinitely apart ($1/d = 0$), the interaction vanishes and Eq. (11) reduces to the shape anisotropy of the isolated NTs (NW).

As seen in Fig. 2 (c), the effective anisotropy energy depends sensibly on the value of the NT wall thickness (β). For $\beta < 0.8$, there is a critical distance between NTs where the effective anisotropy energy passes through zero and becomes negative at shorter distances. The change of sign in the anisotropy energy indicates that the easy axis magnetization rotates from the NT axis to its normal when the strength of the interaction field overcomes the shape anisotropy field. This effect is known as the magnetization easy axis reorientation transition (EART).

The other interesting feature shown in Fig. 2 is that this reorientation transition is inhibited when the wall thickness is small, $\beta \geq 0.8$. Furthermore, for nanotube arrays, the magnetization perpendicular to the axis, or hard axis, is not favorable energetically. These points are addressed in detail in the following sections.

To obtain an analytic expression for the effective magnetic anisotropy [Eq. (11)], the approximate expression for N_{wz} proposed by Sato and Ishii[47], Eq. (10), has been used. To test the validity of the results obtained with this approximation, we have compared these results with those obtained using the rigorous expression for N_{wz} derived by Tandon et al.,[49] in Eq. (8) considering the particular case of NW arrays ($\beta = 0$). The results are shown as solid squares in figures 2 (a)-(c). As seen from these curves, the results provided by both expressions show a very good agreement and thus validating the use of Eq. (10).

Equation (11) describes the effective anisotropy of 2D nanocylinder arrays. It is a simple, approachable, and complete analytical expression that combines naturally the shape

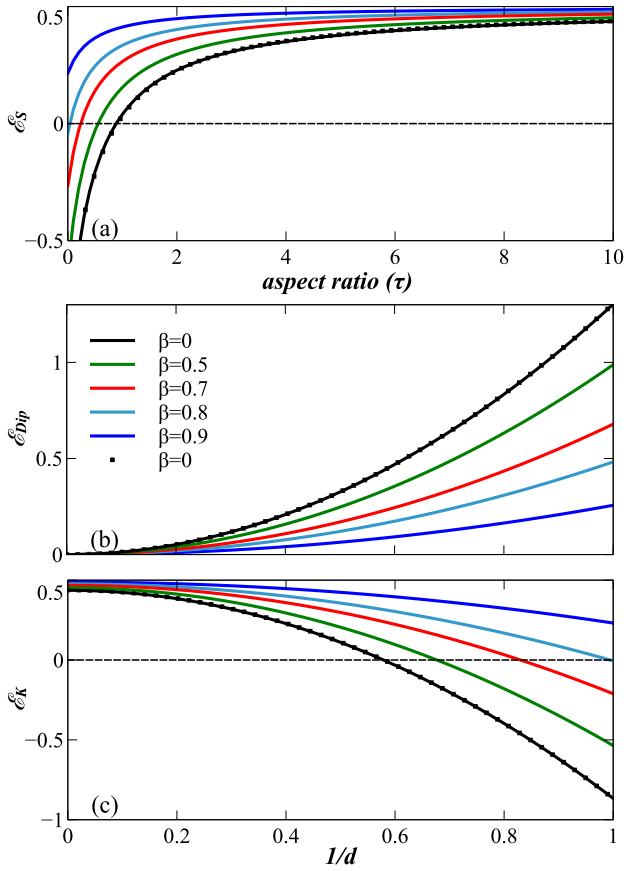

Fig. 2 (a) Reduced shape anisotropy energy $\mathscr{E}_S$ as a function of their aspect ratio, (b) reduced dipolar interaction energy $\mathscr{E}_{Dip}$ and (c) reduced magnetic anisotropy energy $\mathscr{E}_K$ as a function of the reduced reciprocal center to center distance $1/d = \phi/D$ for an array of NTs with aspect ratio $\tau = 10$, for different values of β. Filled squares corresponds to the results obtained using the rigorous expression for N_{wz} derived by Tandon et al.,[49] and Eq. (8)

anisotropy of the cylinder and the dipolar interaction between them as a function of the geometrical parameters of the system. It is, therefore, interesting to compare our model with others used in the literature for the study of these cylindrical systems. As mentioned previously, at present, there are models capable of providing an accurate account for these two effects; however, such models, typically micromagnetic[29,32,33,50–52], require intensive computing resources and depending on the approximations used, the degree of complexity in the programming can vary. However, there is a simple analytical model for nanowires that frequently has been used[41,42,53–57]. In this case, the effective field (in CGS units) is given by,

$$H_{eff} = 2\pi M_s - \frac{6.3 M_s \pi r_2^2 h}{D^3} \tag{14}$$

Writing this expression as a reduced effective anisotropy, we have to divide by $4\pi M_s$. Moreover, by noting that $r_2^2 h/D^3 = \tau/(4d^3)$, the following expression is obtained;

$$\mathscr{E}_K = \frac{1}{2} - \frac{0.393\tau}{d^3} \tag{15}$$

In principle, this expression corresponds to Eq. (11). Com-

View Article Online
DOI: 10.1039/D0CP00808G

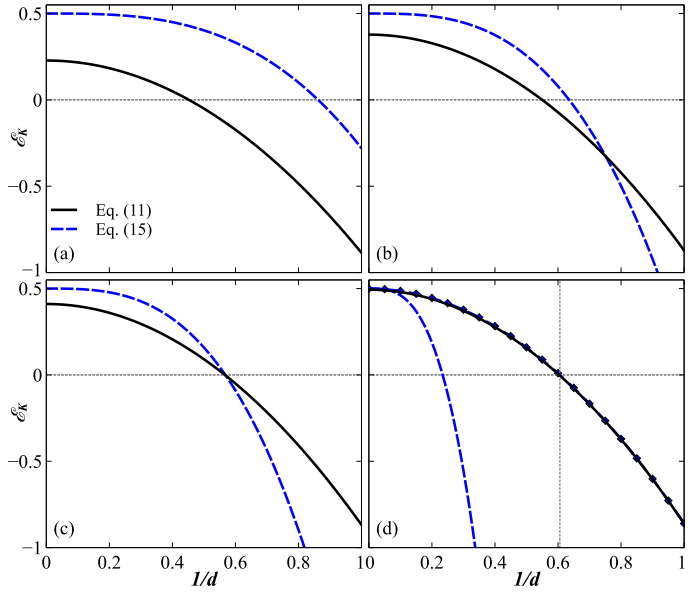

Fig. 3 Comparison of the reduced magnetic anisotropy energy $\mathscr{E}_K$ as a function of the reciprocal reduced center to center distance $1/d = \phi/D$ for an array of NWs with aspect ratio (a) $\tau = 2$, (b) $\tau = 5$, (c) $\tau = 7$ and (d) $\tau = 100$, calculated using Eq. (11) [continuos line] and Eq. (15) [dashed blue line]. For (d) $\tau = 100$, the squares correspond to the values obtained with Eq. (12) for the limiting case of very high aspect ratio NWs and the horizontal dotted line indicates the reduced reciprocal center to center distance for the critical packing fraction of very tall NWs.

paring both expressions, both contain two terms, the first one corresponding to the shape anisotropy while the second one accounts for the inter-wire dipolar interaction; in both cases, the interaction term is preceded by a negative sign implying an antiferromagnetic dipolar interaction. However, there is a clear problem with Eq. (15) as the first term implies an infinitely tall wire, while the dipolar interaction term is proportional to the wire aspect ratio, which will lead to a non-physical result when $\tau \to \infty$. While for low aspect ratio cylinders, Eq. (15) clearly will overestimate the contribution of the shape anisotropy. Moreover, Eq. (15) should also correspond to Eq. (12) for the case of very tall cylinders. Comparing these expressions, we see that the first term is the same, but the second term is not. In Eq. (12) the dipolar interaction only depends on the distance between cylinders while in Eq. (15) this term also depends on the aspect ratio. To further compare Eqs. (11) and (15), figure 3 shows the total reduced energy as a function of the reduced center-to-center distance for a hexagonal 2D array of wires (β=0) with different aspect ratios (τ= 2, 5, 7 and 100) using these equations. As seen in Fig. 3, regardless of the cylinder aspect ratio, the curves provided by each expression differ significantly. However, they both provide a correct trend with the reciprocal center-to-center distance. Indeed, the energy has its maximum when the cylinders are far apart [$(1/d)$=0], and the interaction vanishes, while as the cylinders are brought together [$(1/d)$ goes to 1], the interaction term increases, leading to the reduction of the energy and finally overcoming the shape anisotropy which, as mentioned before, corresponds to the EART.

However, as seen in Fig. 3 (a), (b) and (c), the limiting value of the energy when the cylinders are far apart [$(1/d)$=0] is always the same (1/2) regardless of the aspect ratio. Thus overestimating the contribution of the shape anisotropy, which in combination with the linear dependence of the interaction term on the cylinder aspect ratio leads to an incorrect description of the interplay between these two contributions to the energy.

To provide further evidence of the inconsistency of Eq. (15) figure SI1 (see supplementary information) shows the total reduced magnetic anisotropy energy as a function of the reduced center-to-center distance calculated using Eq. (11) and modifying the first term of Eq. (15). As inferred from the variation of the critical distance at which the reduced energy is zero the results obtained with Eq. (15) show that this distance increases as the cylinder aspect ratio decreases, which is incorrect, as one expects that as the aspect ratio decreases, the shape anisotropy also decreases and thus requiring a lower interaction field to cancel the shape anisotropy. So that for smaller aspect ratios, the shape anisotropy cancels out at larger inter-cylinder distances, as predicted by Eq. (15).

Finally, as seen in Fig. 3 (d) for very tall cylinders, both expressions yield the same (and correct) limiting value ($\mathscr{E}_K$=1/2) when the distance between them increases [$(1/d)$=0] and the reduced energy decreases as the distance between them is reduced. However, due to the linear dependence on the aspect ratio of the interaction term in Eq. (15) the interaction is sensibly overvalued leading to a very fast decrease of the reduced energy and thus largely overestimating the critical distance where the reduced energy vanishes. Moreover, comparing Eqs. (11) and (12), the latter shown as solid squares, for very tall cylinders, we see that both expressions yield the same results and the critical distance is consistent with the known value corresponding to P=1/3 or $(1/d)$=0.606 for an hexagonal 2D array[29,40] which is shown as a vertical dotted line.

4 Easy axis reorientation transition induced by the dipolar interaction

As already pointed out, the results shown in Figure 2 (c) for the anisotropy energy evidence a change of sign of this energy as the distance between NTs is reduced and also the inhibition of this effect above a certain value of the reduced inner radii. The change of sign of the anisotropy energy reflects the rotation of the easy axis magnetization as a function of distance between tubes occurs when the second term of Eq. (8) becomes higher than the first. This is when the dipolar interaction field energy exceeds that of the shape anisotropy. This EART is well known, and it has been observed in different systems such as cylindrical nanowires[29,33,40,41,44,52,56–73], circular dots[74,75], and ellipses[76].

The EART depends on the distance between NTs or the packing fraction and takes place when the MAE vanishes. Taking $\mathscr{E}_K = 0$ in equation (8) and using $P_t = P_c(1-\beta^2)$, the critical packing is expressed as,

$$P_c = \frac{1}{3}\left[\frac{(1-3N_z)}{(1-N_z)}\right]\left(\frac{1}{1-\beta^2}\right) \qquad (16)$$

which depends only on the NT axial demagnetizing factor (N_z) and the wall thickness (β). Before introducing explicitly the

View Article Online
DOI: 10.1039/D0CP00808G

center-to-center distance, note that the packing fraction is such that $0 \leq P_c \leq 1$, implying that both terms on the right side in Eq. (16) must be positive. The first term (in square brackets) depends only on the demagnetizing factor, and it will only be positive if $0 \leq N_z < 1/3$. This condition implies that the easy axis of a single non-interacting NT lies along the z-axis. This is a necessary condition for the EART to take place. Notice that if the easy axis is perpendicular to the NT axis, $N_z > 1/3$ and $P_c < 0$ implying that the easy axis will not rotate. On the other hand, the NT wall thickness is such that $0 \leq \beta \leq 1$, so the last term is always positive, but P_c diverges as $\beta \to 1$, which will be discussed below. As a first limiting case, consider Eq. (16) the case of an array of high aspect ratio nanowires, namely, $N_z = 0$ and $\beta = 0$, for these values Eq. (16) leads to $P_c = 1/3$, which is the well-known value of the critical packing fraction for a 2D array of very tall nanowires[29,40].

Using Eq. (1) to introduce the dependence on the reduced center-to-center distance and Eqs. (9) and (10) for N_z in Eq. (16) we obtain the following expression for the critical aspect ratio (τ_c) as a function of the reduced center-to-center distance and the reduced inner radii (β),

$$\tau_c = \frac{\sqrt{\pi}}{4}\left(\frac{\frac{\pi\sqrt{3}}{2d^2}\left(1-\beta^2\right)-3}{\frac{\pi\sqrt{3}}{2d^2}\left(1-\beta^2\right)-1}\left(1-\beta^2\right)-1\right) \qquad (17)$$

For the particular case of a single non-interacting NT, $d \to \infty$, this expression reduces to Eq. (13), as expected. Equation (17) allows tracing the easy axis reorientation transition diagram for different values of d and β. Consider first the particular case of NW arrays ($\beta = 0$), the corresponding EART diagram, $\tau_c(d)$, is shown as a continuous line in Figure 4 (a). Here the upper-right side of the curve indicates the easy axis is parallel to the long axis (z-axis) while points in the lower-left side of the curve have their easy axis along the short axis (xy-plane). Indeed, for low aspect ratios, the shape anisotropy of a single wire is small, and it requires smaller interaction field values to reverse the easy axis. So even at large distances, the easy axis is reversed by the interaction field. For high aspect ratios, the shape anisotropy is stronger, and the distance between wires has to be reduced in order for the interaction field to overwhelm the shape anisotropy. For the liming case of infinitely tall NWs, the critical packing fraction P_c=1/3[29,40,77], which corresponds to a center to center distance of d=1.65 that is shown in Fig. 4 (a) as a vertical dashed line. The EART in NW arrays has been reported by numerous studies[29,33,40,41,44,52,56–73]. From these studies, we have taken the coordinates (aspect ratio and center-to-center distance) and plotted them in the EART diagram shown in Fig. 4 (a). Only those studies that provide all the required data (wire diameter, height, and center-to-center distance) were considered[44,52,59–64]. As seen in Fig. 4 (a), the prediction of the easy axis orientation in magnetic NW arrays obtained with Eq. (17) is consistent with the experimental findings of previous studies. However, there are a couple of coordinates as well as other studies whose results do not match with the prediction of Eq. (17). This can be attributed to several factors, such as experimental uncertainty, dispersion of geometrical parameters, or even geometrical deviations with respect to the perfect circular cylinder shape. In supplementary

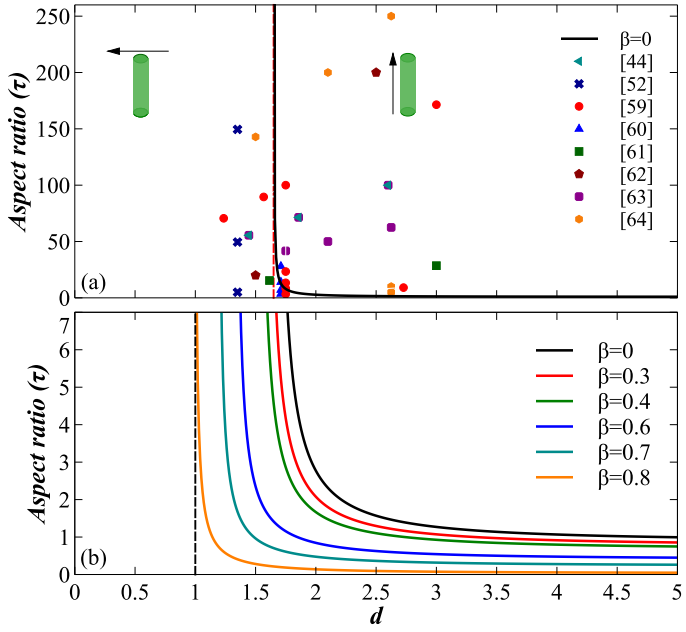

Fig. 4 (a) EART diagram calculated with Eq.(17) and $\beta = 0$, and (b) effective anisotropy diagrams calculated for different values of β.

information, we provide a table with details of each point shown in the figure, as well as those points that do not coincide.

The EART diagrams for NT arrays with different reduced inner radii calculated using Eq. (17) are shown in Figure 4 (b). Each of these curves provides the values of NT aspect ratio and distance between them where the effective magnetic anisotropy vanishes, this is, where the assembly is isotropic. For all cases, the upper right region corresponds to the case where the magnetic anisotropy easy axis is along the cylinder axis, whereas the lower left region contains those cases where the easy axis is perpendicular to the cylinder axis.

As seen in the figure, the value of the internal radii has a strong effect on the conditions that lead to the easy axis reorientation. As mentioned previously (Fig. 2), at a fixed aspect ratio; increasing the internal radii leads simultaneously to (a) an increase of the shape anisotropy of a single tube [Fig. 2 (a)], and (b) a decrease of the value of the interaction field [Fig. 2 (b)]. As seen in Figure 4 (b), at a fixed intertube distance, the critical aspect ratio decreases as β increases. In contrast at a fixed aspect ratio, the critical inter-tube distance required to reach the isotropic point is smaller as β increases.

This implies that by decreasing the tube wall thickness, the NTs can be brought closer, and above a given internal radii, the EART is frustrated. The easy axis is blocked along the cylinder axis even if the center to center distance approaches its lowest value d=1 (when the tubes come in contact). This limiting case is shown as a vertical dashed line in Fig. 4 (b), as seen in the figure, the EART is not reached when $\beta = 0.8$ and the aspect ratio increases. This is consistent with the results shown in Fig. 2 (c) where it was also observed that for $\beta \geq 0.8$ the anisotropy energy does not reach zero even for $d = 1$. However, as seen for $\beta = 0.8$ in Fig. 4 (b), the frustration of the EART also depends on the NT aspect ratio. Indeed, in this case ($\beta = 0.8$) for low aspect ratios,

View Article Online
DOI: 10.1039/D0CP00808G

the EART does take place. This suggests that for a given value of the inner radii, there is a critical NT aspect ratio above which the EART will be frustrated. This relation follows directly from equation (17) by making $d = 1$. However, some considerations are required since, as explained before, all the variables are bounded, or they must follow restrictions. The first one is that for the EART to take place $0 \leq N_z < 1/3$ and by Eqs. (9) and (10), it depends on both NT aspect ratio and inner radii, which are such that $\tau \geq 0$ and $0 \leq \beta < 1$, respectively.

Taking these restrictions into account, Figure 5 shows the variation of the critical aspect ratio (τ_c) as a function of the inner radii. Due to the restrictions that $0 \leq N_z < 1/3$ and $\tau_c \geq 0$, the inner radii has an upper bound at $\beta \approx 0.9$. While close to $\beta = 0.8$, τ_c increases. To analyze the limit of infinitely tall NTs, we use Eq. (16) for $N_z = 0$ and solve for β, namely

$$\beta = \sqrt{1 - \frac{1}{3P_c}}, \tag{18}$$

then, using Eq. (1) with $d = 1$, we obtain $\beta = 0.79529$, which corresponds to the lowest value of the inner radii for which the frustration of the EART is observed and this for the case of infinitely tall NTs. This lower limit is shown as a vertical dashed line in Figure 5. This curve defines the coordinates (β, τ_c) where the magnetic anisotropy vanishes when $d = 1$, so that in the upper right side of the curve the EART will be frustrated and inversely, in the lower-left side the EART will take place.

Finally, these results have been obtained considering only the shape anisotropy and the dipolar interaction field, both of magnetostatic origin. However, other contributions to the energy, originating from other effects, can also be considered by including the appropriate additive terms. This would be the case for the magnetocrystalline or magneto-elastic anisotropies, related to the spin-orbit coupling or other interaction effects. Furthermore, as a mean-field model, it applies best to systems containing a very large number of particles, so that the average values of their main properties are representative. In this sense, the model applies to NW and NT arrays as those typically obtained by electrodepostion into nanoporous templates, with diameters ranging from 10-300 nm and heights between 5-100 μm with packing fractions below 35-40% and densities of 10^7-10^{11} wires (tubes) per square centimeter. For these large particle volumes, temperature driven effects are not expected to play any important role. Finally, this macroscopic model is not expected to describe accurately the properties of smaller atomic scale wires or tubes,[78–83] where first neighbor exchange interactions or stronger effects related to the spin-orbit coupling play a more prominent role.

5 Conclusion

A simple mean-field analytical model was presented for the magnetostatic energy in 2D arrays of cylinders, namely wires and tubes. The model is expressed in terms of all the geometrical parameters of the systems and due to its simplicity, calculations can be done varying each parameter using simple software and without requiring specialized hardware. For the particular case of NW arrays, the model provides predictions that are in good agreement with those obtained previously, namely the competition between shape anisotropy and the dipolar interaction. For NTs, the model also shows a very sensitive dependence on the NT wall thickness. Specifically, an increase of the shape anisotropy of individual tubes and a reduction of the inter-tube dipolar interaction as the wall thickness decreases. An analytical expression has been obtained for the easy axis reorientation transition induced by the dipolar interaction. The results obtained for NWs agree very well with experimental results reported in previous studies. For NTs, an interesting property predicted by the model is that the easy axis reorientation transition can be inhibited or frustrated by reducing the tube wall thickness even when the inter-tube distance is reduced to its minimum allowable value. This property is of great interest in 2D magnetic arrays with perpendicular anisotropy in which the density is desired to increase.

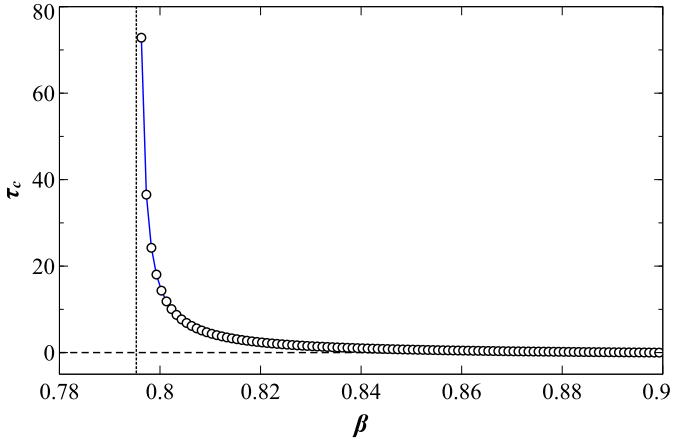

Fig. 5 Critical aspect ratio (τ_c) as a function of the inner radii. The vertical dashed line corresponds to the limiting value of the inner radii, $\beta = 0.79529$, when the NT aspect ratio is infinite ($N_z = 0$).

Conflicts of interest

The authors declare that there are no conflicts to declare.

Acknowledgements

This study received financial support from CONACYT Ciencia Básica grant 286626.

References

1 R. L. Stamps, S. Breitkreutz, J. Åkerman, A. V. Chumak, Y. Otani, G. E. W. Bauer, J.-U. Thiele, M. Bowen, S. A. Majetich, M. Kläui, I. L. Prejbeanu, B. Dieny, N. M. Dempsey and B. Hillebrands, *Journal of Physics D: Applied Physics*, 2014, **47**, 333001.

2 D. Sander, S. O. Valenzuela, D. Makarov, C. H. Marrows, E. E. Fullerton, P. Fischer, J. McCord, P. Vavassori, S. Mangin, P. Pirro, B. Hillebrands, A. D. Kent, T. Jungwirth, O. Gutfleisch, C. G. Kim and A. Berger, *Journal of Physics D: Applied Physics*, 2017, **50**, 363001.

3 A. Fernández-Pacheco, R. Streubel, O. Fruchart, R. Hertel, P. Fischer and R. P. Cowburn, *Nature Communications*, 2017, **8**, 15756.

4 P. Fischer, D. Sanz-Hernández, R. Streubel and A. Fernández-

View Article Online
DOI: 10.1039/D0CP00808G

Pacheco, *Applied Physics Letters Materials*, 2020, **8**, 010701.
5 I. Stanković, M. Dašić, J. A. Otálora and C. García, *Nanoscale*, 2019, **11**, 2521–2535.
6 A. May, M. Hunt, A. V. D. Berg, A. Hejazi and S. Ladak, *Communications Physics*, 2019, **2**, year.
7 R. A. Bennett, H. A. Etman, H. Hicks, L. Richards, C. Wu, M. R. Castell, S. S. Dhesi and F. Maccherozzi, *Nano Letters*, 2018, **18**, 2365–2372.
8 G. E. W. Bauer, E. Saitoh and B. J. van Wees, *Nature Materials*, 2012, **11**, 391 – 399.
9 S. R. Boona, R. C. Myers and J. P. Heremans, *Energy & Environmental Science*, 2014, **7**, 885.
10 T. da Câmara Santa Clara Gomes, F. A. Araujo and L. Piraux, *Science Advances*, 2019, **5**, eaav2782.
11 P. D. McGary, L. Tan, J. Zou, B. J. H. Stadler, P. R. Downey and A. B. Flatau, *Journal of Applied Physics*, 2006, **99**, 08B310.
12 S. B. J. Atulasimha, *Nanomagnetic and Spintronic Devices for Energy-Efficient Memory and Computing*, John Wiley and Sons, 2016.
13 S. H. Skjærvø, C. H. Marrows, R. L. Stamps and L. J. Heyderman, *Nature Reviews Physics*, 2019, 13–28.
14 Y. Bao, T. Wen, A. C. S. Samia, A. Khandhar and K. M. Krishnan, *Journal of Materials Science*, 2015, **51**, 513–553.
15 I. Orue, L. Marcano, P. Bender, A. García-Prieto, S. Valencia, M. A. Mawass, D. Gil-Cartón, D. A. Venero, D. Honecker, A. García-Arribas, L. F. Barquín, A. Muela and M. L. Fdez-Gubieda, *Nanoscale*, 2018, **10**, 7407–7419.
16 O. S. Pak, W. Gao, J. Wang and E. Lauga, *Soft Matter*, 2011, **7**, 8169.
17 L. Khanna, N. Verma and S. Tripathi, *Journal of Alloys and Compounds*, 2018, **752**, 332–353.
18 J. G. Wan, X. W. Wang, Y. J. Wu, M. Zeng, Y. Wang, H. Jiang, W. Q. Zhou, G. H. Wang and J.-M. Liu, *Applied Physics Letters*, 2005, **86**, 122501.
19 Z. Hua, P. Yang, H. Huang, J. Wan, Z.-Z. Yu, S. Yang, M. Lu, B. Gu and Y. Du, *Materials Chemistry and Physics*, 2008, **107**, 541–546.
20 H. Zheng, *Science*, 2004, **303**, 661–663.
21 A. Fert and L. Piraux, *Journal of Magnetism and Magnetic Materials*, 1999, **200**, 338.
22 Y. Ye and B. Geng, *Critical Reviews in Solid State and Materials Sciences*, 2012, **37**, 75–93.
23 *Magnetic Nano- and Microwires*, ed. M. Vázquez, Woodhead Publishing, 2015.
24 M. Staňo and O. Fruchart, in *Handbook of Magnetic Materials*, ed. E. Brück, Elsevier, 2018, vol. 27, ch. 3, pp. 155–267.
25 L. Piraux, A. Encinas, L. Vila, S. Mátéfi-Tempfli, M. Mátéfi-Tempfli, M. Darques, F. Elhoussine and S. Michotte, *Journal of Nanoscience and Nanotechnology*, 2005, **5**, 372.
26 M. Darques, A. Encinas, L. Vila and L. Piraux, *Journal of Physics D: Applied Physics*, 2004, **37**, 1411.
27 Y. Velázquez-Galván, J. de la Torre Medina, L. Piraux and A. Encinas, *Journal of Magnetism and Magnetic Materials*, 2020, **497**, 165992.
28 R. Hertel, *Journal Applied Physics*, 2001, **90**, 5752.
29 F. Zighem, T. Maurer, F. Ott and G. Chaboussant, *Journal of Applied Physics*, 2011, **109**, 013910.
30 Y. P. Ivanov and O. Chubykalo-Fesenko, in *Magnetic Nano- and Microwires: Design, Synthesis, Properties and Applications*, ed. M. Vázquez, Woodhead Publishing, 2015, ch. 14, p. 423.
31 Y. L. Li, S. L. Tang, R. Xie, Y. Wang, M. Yang, J. L. Gao, W. B. Xia and Y. W. Du, *Applied Physics Letters*, 2012, **100**, 052402.
32 C. Garcia, W. O. Rosa, J. Garcia, V. M. Prida, B. Hernando, J. A. López, P. Vargas and C. A. Ross, *The Journal of Physical Chemistry C*, 2018, **122**, 5124–5130.
33 M. Sharma, A. Basu and B. K. Kuanr, *Journal of Magnetism and Magnetic Materials*, 2019, **476**, 234–242.
34 J. Escrig, S. Allende, D. Altbir and M. Bahiana, *Applied Physics Letters*, 2008, **93**, 023101.
35 I. S. Jacobs and C. P. Bean, *Physical Review*, 1955, **100**, 1060–1066.
36 W. Chen, S. Tang, M. Lu and Y. Du, *Journal of Physics: Condensed Matter*, 2003, **15**, 4623 – 4630.
37 E. Padrón-Hernández, S. M. Rezende and A. Azevedo, *Journal of Applied Physics*, 2008, **103**, 07D506.
38 J. Gong, S. Yang, C. Han, W. Guan, Y. Wang, B. Gao, D. Wang, X. Song, Z. Sun and M. Xu, *Journal of Applied Physics*, 2012, **111**, 063912.
39 J. Wang, S. Yang, J. Gong, M. Xu, M. Adil, Y. Wang, Y. Zhang, X. Song and H. Zeng, *Physical Chemistry Chemical Physics*, 2015, **17**, 10250.
40 A. Encinas-Oropesa, M. Demand, L. Piraux, I. Huynen and U. Ebels, *Physical Review B*, 2001, **63**, 104415.
41 G. J. Strijkers, J. H. J. Dalderop, M. A. A. Broeksteeg, H. J. M. Swagten and W. J. M. de Jonge, *Journal of Applied Physics*, 1999, **86**, 5141.
42 M. Grimsditch, Y. Jaccard and I. K. Schuller, *Physical Review B*, 1998, **58**, 11539 – 11543.
43 Y. Velázquez-Galván, J. M. Martínez-Huerta, J. de la Torre Medina, Y. Danlée, L. Piraux and A. Encinas, *Journal of Physics: Condensed Matter*, 2014, **26**, 026001.
44 E. V. Tartakovskaya, M. Pardavi-Horvath and M. Vázquez, *Journal of Magnetism and Magnetic Materials*, 2010, **322**, 743–747.
45 *GeoGebra webpage*, 2020, https://www.geogebra.org/.
46 J. M. Martínez-Huerta, J. de la Torre Medina, L. Piraux and A. Encinas, *Journal of Physics: Condensed Matter*, 2013, **25**, 226003.
47 M. Sato and Y. Ishii, *Journal of Applied Physics*, 1989, **66**, 983.
48 B. Nam, J. Kim and K. Ki Hyeon, *Journal of Applied Physics*, 2012, **111**, 07E347.
49 S. Tandon, M. Beleggia, Y. Zhu and M. D. Graef, *Journal of Magnetism and Magnetic Materials*, 2004, **271**, 9–26.
50 Y. Peng, M. Yue, H. Li, Y. Li, C. Li, H. H. Xu, Q. Wu and W. Xi, *IEEE Transactions on Magnetics*, 2018, **54**, 1–5.
51 O. Albrecht, R. Zierold, S. Allende, J. Escrig, C. Patzig, B. Rauschenbach, K. Nielsch and D. Görlitz, *Journal of Applied Physics*, 2011, **109**, 093910.

View Article Online
DOI: 10.1039/D0CP00808G

52 M. Ciureanu, F. Beron, L. Clime, P. Ciureanu, A. Yelon, T. A. Ovari, R. W. Cochrane, F. Normandin and T. Veres, *Electrochimica Acta*, 2005, **50**, 4487.

53 G. Han, B. Zong and Y. Wu, *IEEE Transactions on Magnetics*, 2002, **38**, 2562–2564.

54 G. C. Han, B. Y. Zong, P. Luo and Y. H. Wu, *Journal of Applied Physics*, 2003, **93**, 9202–9207.

55 A. Ghaddar, F. Gloaguen, J. Gieraltowski and C. Tannous, *Physica B: Condensed Matter*, 2011, **406**, 2046–2053.

56 S.-G. Cho, B. Yoo, K. H. Kim and J. K, *IEEE Transactions on Magnetics*, 2010, **46**, 420.

57 M. S. Salem and K. Nielsch, *Materials Science and Engineering B*, 2017, **223**, 120–124.

58 M. Lederman, R. O'Barr and S. Schultz, *IEEE Transactions on Magnetics*, 1995, **31**, 3793–3795.

59 G. Kartopu, O. Yalçin, K. L. Choy, R. Topkaya, S. Kazan and B. Aktaş, *Journal Applied Physics*, 2011, **109**, 033909.

60 B. Das and K. Mandal, *Journal of Applied Physics*, 2008, **103**, 031908.

61 M. Vázquez and L. G. Vivas, *Physica Status Solidi B*, 2011, **248**, 2368.

62 S. Khalid, R. Sharif and Z. H. Shah, *Surface Review and Letters*, 2016, **23**, 1650024.

63 M. Pardavi-Horvath, P. E. Si, M. Vazquez, W. O. Rosa and G. Badini, *Journal of Applied Physics*, 2008, **103**, 07D517.

64 G. Kartopu, O. Yalçin, M. Es-Souni and A. C. Basaran, *Journal of Applied Physics*, 2008, **103**, 093915.

65 M. Vázquez, K. Pirota, M. Hernández-Vélez, V. M. Prida, D. Navas, R. Sanz and F. Batallán, *Journal of Applied Physics*, 2011, **95**, 6642.

66 S. Shamaila, D. P. Liu, R. Sharif, J. Y. Chen, H. R. Liu and X. F. Han, *Applied Physics Letters*, 2009, **94**, 203101.

67 J. Mallet and K. Yu-Zhang, *Applied Physics Letters*, 2004, **84**, 3900.

68 P. M. Paulus, F. Luis, M. Kröll, G. Schmid and L. J. de Jongh, *Journal of Magnetism and Magnetic Materials*, 2001, **224**, 180–196.

69 J. Rivas, A. K. M. Bantu, G. Zaragoza, M. C. Blanco and M. A. López-Quintela, *Journal of Magnetism and Magnetic Materials*, 2002, **249**, 220–227.

70 L. V. Thiem, T. le Tu and M. H. Phan, *Sensors*, 2015, **15**, 5687–5696.

71 S. Goolaup, N. Singh, A. O. Adeyeye, V. Ng and M. B. A. Jalil, *The European Physical Journal B - Condensed Matter and Complex Systems*, 2005, **44**, 259–264.

72 F. Ebrahimi, F. Ashrafizadeh and S. R. Bakhshi, *Journal of Alloys and Compounds*, 2016, **656**, 237–244.

73 A. Encinas-Oropesa, M. Demand, L. Piraux, U. Ebels and I. Huynen, *Journal of Applied Physics*, 2001, **89**, 6704–6706.

74 K. Y. Guslienko, *Applied Physics Letters*, 1999, **75**, 394–396.

75 K. Y. Guslienko, S.-B. Choe and S.-C. Shin, *Applied Physics Letters*, 2000, **76**, 3609–3611.

76 S. Jain, A. O. Adeyeye and N. Singh, *Nanotechnology*, 2010, **21**, 285702.

77 L.-P. Carignan, C. Lacroix, A. Ouimet, M. Ciureanu, A. Yelon and D. Ménard, *Journal of Applied Physics*, 2007, **102**, 023905.

78 D. Hashemi, M. J. Waters, W. Hergert, J. Kieffer and V. S. Stepanyuk, *Nanomaterials*, 2020, **10**, 159.

79 H. Hashemi, A. Bregman, H. S. Nabi and J. Kieffer, *RSC Advances*, 2016, **6**, 108948.

80 H. Hashemi, G. Fischer, W. Hergert and V. S. Stepanyuk, *Journal Applied Physics*, 2010, **107**, 09E311.

81 C. F. Hirjibehedin, C. P. Lutz and A. J. Heinrich, *Science*, 2006, **312**, 1021.

82 P. Gambardella, A. Dallmeyer, K. M. M. C. Malagoli, W. Eberhardt, K. Kern and C. Carbone, *Nature*, 2002, **416**, 301.

83 J. Shen, R. Skomski, M. Klaua, H. Jenniches, S. S. Manoharan and J. Kirschner, *Physical Review B*, 1997, **56**, 2340.

Inhibition of the easy axis reorientation transition in nanotubes when the tube wall thickness decreases